Indonesian Journal of Electrical Engineering and Informatics (IJEEI)
Vol. 11, No. 3, September 2023, pp. 791~804
ISSN: 2089-3272, DOI: 10.52549/ijeei.v11i3.4463

Examination on the Denoising Methods for Electrical and Acoustic Emission Partial Discharge Signals in Oil

Ahmad Hafiz Mohd Hashim[1], Norhafiz Azis[2], Jasronita Jasni[3], Mohd Amran Mohd Radzi[4], Masahiro Kozako[5], Mohamad Kamarol Mohd Jamil[6], and Zaini Yaakub[7]

[1,2,3,4]Advanced Lightning, Power and Energy Research Centre (ALPER), Faculty of Engineering, Universiti Putra Malaysia
[1]Electrical and Electronic Department, German-Malaysian Institute, Selangor, Malaysia
[2]Institute of Nanoscience and Nanotechnology (ION2), Universiti Putra Malaysia, Selangor, Malaysia
[5]Department of Electrical and Electronic Engineering, Kyushu Institute of Technology, Kitakyushu-shi, Fukuoka, Japan
[6]School of Electrical and Electronic Engineering, Universiti Sains Malaysia, Penang, Malaysia
[7]Hyrax Oil Sdn. Bhd., Selangor, Malaysia

Article Info

Article history:

Received Jan 22, 2023
Revised Sep 10, 2023
Accepted Sep 24, 2023

Keyword:

Partial discharge
Denoising
Moving average
Finite impulse response
Low pass filter
High pass filter
Discrete wavelet transform

ABSTRACT

Partial discharge (PD) measurements either through electrical or acoustic emission approaches can be subjected to noises that arise from different sources. In this study, the examination on the denoising methods for electrical and acoustic emission PD signal is carried out. The PD was produced through needle-plane electrodes configuration. Once the voltage reached to 30 kV, the electrical and acoustic emission PD signals were recorded and additive white Gaussian noise (AWGN) was introduced. These signals were then denoised using moving average (MA), finite impulse response (FIR) low/high-pass filters, and discrete wavelet transform (DWT) methods. The denoising methods were evaluated through ratio to noise level (RNL), normalized root mean square error (NRMSE) and normalized correlation coefficient (NCC). In addition, the computation times for all denoising methods were also recorded. Based on RNL, NRMSE and NCC indexes, the performances of the denoising methods were analyzed through normalization based on the coefficient of variation (C_v). Based on the current study, it is found that DWT performs well to denoise the electrical PD signal based on the RNL and NRMSE C_v index while MA has a good denoising NCC and computation time C_v index for acoustic emission PD signal.

Corresponding Author:

Norhafiz Azis,
Advanced Lightning, Power and Energy Research Centre (ALPER),
Faculty of Engineering, Universiti Putra Malaysia,
43400 UPM Serdang, Selangor, Malaysia
Email: norhafiz@upm.edu.my

1. INTRODUCTION

Partial discharge (PD) evaluation is one of the most common non-destructive techniques to evaluate the condition of insulation system in high voltage equipment [1, 2]. Generally, PD can be detected through electrical approach whereby concurrently it can produce acoustic emission waves that travel through the oil and paper insulations as well as within the experimental or in-service transformer tank [3]. Electrical PD measurement is able to provide the direct information on the condition of the insulation. However, it can be subjected to noises arise from the electrical system. Acoustic emission PD has several advantages which include the ease of use and immunity to electrical noises from the system [4]. Nevertheless, acoustic emission PD still can be subjected to nearby mechanical noises. Broadband noise and noise spectrum are 2 forms of noises that might be present during the PD measurement. White noise or measurement-related noise is an

example of broadband noise. Environmental noise, which include narrowband, periodic pulse-shaped and radio transmissions noises can contribute to the occurrence of discrete spectral interference (DSI) [5-8].

Electrical and acoustic emission PD signals can be denoised whereby the degree of error level, retained shape and correlation can be examined [9, 10]. Wavelet filtering and cross-correlation are among the common denoising methods that can be used to process the electrical and acoustic emission PD signals [11]. Moving average (MA) is able to reduce between 10% and 50% interference in acoustic emission PD signal [12]. The acoustic emission PD signal detection process can be accelerated using MA and the analysis can be carried in time domain [13-15]. Principle component analysis (PCA) denoised electrical PD through reduction of the number of energy levels that is associated with each of the decomposition levels. PCA standardizes the input data by subtraction of the mean for each of the dimensions to obtain a centred observation by zero mean and unity variance [16, 17].Previous study implements discrete wavelet transform (DWT) with Daubechies finite-length or mother wavelet of 20 to denoise acoustic emission PD signal [18]. Low-pass filter (LPF) and high-pass filter (HPF) are categorized under finite-duration impulse response (FIR), which are able to cut-off frequency that influences the acoustic emission PD signal between 16 kHz and 700 kHz [19]. LPF and HPF are also part of DWT that are used to perform decomposition of electrical PD signal at high level on the tree structure that involves filtering and down-sampling functions [20].

Several studies examine the performance of denoising methods for electrical and acoustic emission PD signals based on signal-to-noise ratio (SNR) [5], [21-23]. There are only few studies that utilize ratio to noise level (RNL), normalized correlation coefficient (NCC) and normalized root mean square error (NRMSE) to evaluate the performance of denoising methods for electrical and acoustic emission PD signals. It is found that the both RNL and NCC are suitable to evaluate the denoising methods for electrical and acoustic emission PD signals [24, 25]. NMRSE is also able to evaluate the denoising method for electrical PD signal [26-28].

The motivation of this paper is to examine the denoising methods for electrical and acoustic emission PD signals. The contribution of this study is the identification of suitable denoising method for electrical and acoustic emission PD signals based on MA, FIR LPF/HPF and DWT. The denoising methods are evaluated through RNL, NCC and NRMSE. The performances of denoising methods are evaluated through coefficient of variation (C_v) and computation time.

2. MATERIALS AND METHODS

2.1. Experiment Setup

The PD measurement was carried out as per IEC 60270 and 61294 [29, 30]. A copper needle-plane electrode configuration with a needle tip radius of 3 µm was utilized to initiate the PD in a 0.025 m³ steel test tank filled with 22 l mineral oil (MO) as shown in Figure 1. The gap distance between electrode tip and plane was set at 50 mm ± 1 mm. The plane electrode is 50 mm in diameter with a 3 mm edge radius. The coordinate of x, y, and z-axes for the electrodes were set at 0.07, 0.08, and 0.18 m respectively.

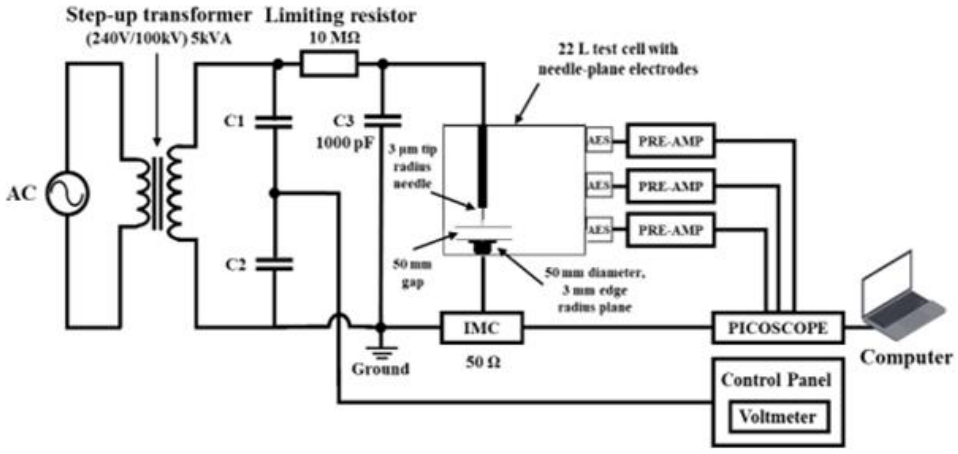

Figure 1. Experimental setup for PD detection.

2.2. Oil Preparation

The uninhibited mineral oil was chosen for this study. The physiochemical properties of MO can be seen in Table 1 [31]. The MO was filtered via a membrane filter with a pore size of 0.2 µm. Next, the oil was dried in an air circulation oven for 48 hours at 85°C.

Table 1. Physiochemical properties of MO

Property	Unit	Test method	Typical value
Density @ 20°C	g/ml	ISO 12185	0.881
Viscosity @ 40°C	cSt	ISO 3104	10.4
Flash point	°C	ISO 2179	145
Pour point	°C	ISO 3106	-60
Interfacial tension	mN/m	ISO 6295	50
Acidity	Mg KOH/g	IEC 6201-1	0.005
Water content	ppm	IEC 60814	20
Appearance	-	ASTM D4176	Clear & Bright

2.3. Partial Discharge Measurement

The electrical and acoustic emission PD signals were measured through Picoscope 4824. The electrical PD signal was measured using an impedance matching circuit (IMC) with a broad 50 Ω input and output impedances. The PD measurement was carried out once the PD inception voltage (PDIV) was achieved. The PD measurement was performed in the range after 30 seconds and 1 minute to ensure stable measurement was obtained [32, 33]. Both electrical and acoustic emission PD signals were acquired simultaneously during the test for the duration of 2.5 ms [34]. The acoustic emission PD signal was acquired through an AE sensor with the frequency ranges from 20 kHz to 180 kHz and 40 dB signal gain pre-amplifier. The voltage was raised at 1 kV/step until 30 kV after the AE sensor was positioned on the test tank's surface. The acoustic emission PD signal was measured as per IEEE Std C57.127-2007 [35]. The sensor coordinates were determined based on the 3-dimensional axes designated as x, y and z [36]. A reference point of (0, 0, 0) was used to define the pre-determined for AE sensor coordinates.

2.4. Denoising Methods

The denoising process was performed once the measured electrical and acoustic emission PD signals were obtained as shown in Figure 2 [37]. A single dimensional additive white Gaussian noise (AWGN) with 0 dB was applied to the measured electrical and acoustic emission PD signals based on Equation (1) where x is the measured signal with AWGN, m is the measured signal, g is the white Gaussian noise and i = (1, 2…N-1) [7], [22].

$$x(i) = m(i) + g(i) \quad (1)$$

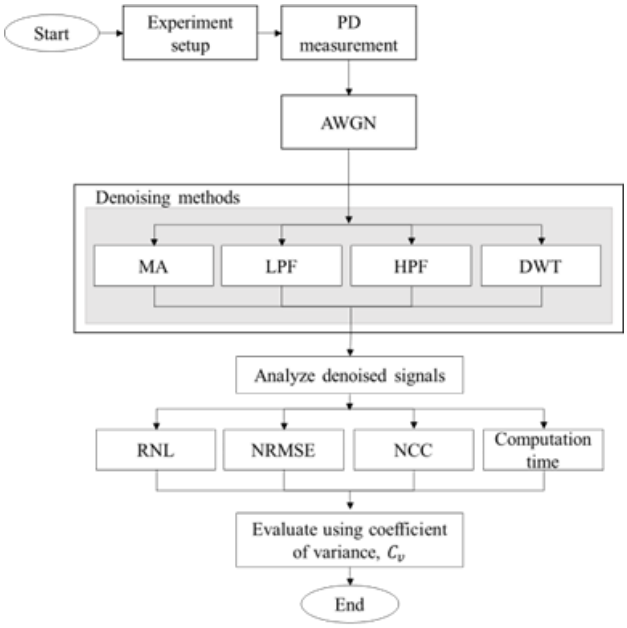

Figure 2. Flow chart for electrical and acoustic emission PD signals denoising methods

An example of AWGN that is included to the electrical and acoustic emission PD signals can be seen in Figures 3 (a) and (b), respectively. In total, 75 random electrical and acoustic emission PD signals with AWGN are examined.

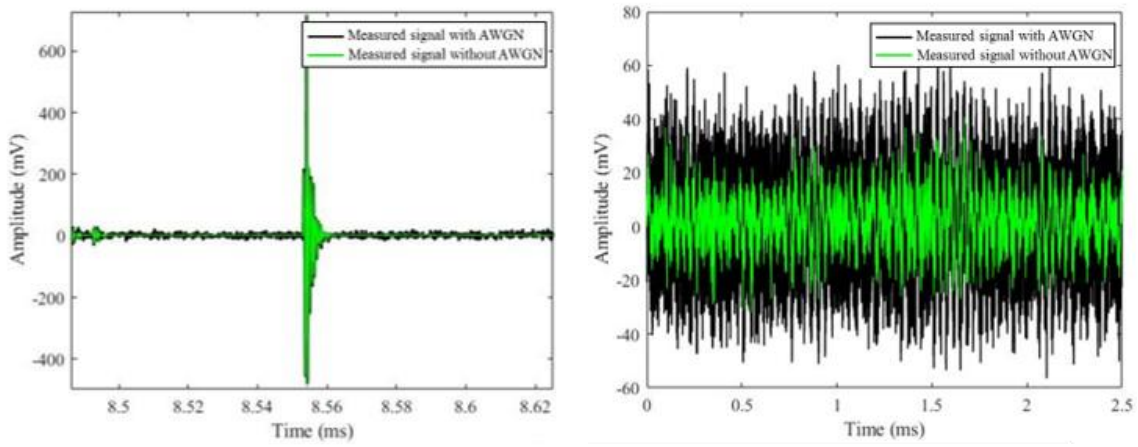

(a) (b)

Figure 3. Measured signal with and without AWGN for (a) electrical and (b) acoustic emission PD signals

2.4.1. Moving Average

The MA superimpose layer window size was defined once it was initialized to zero. At this point, the computation time started to record. Next, random generator for MA was initialized to evaluate its effectiveness to filter the additional noise. The range of window size analyzed in this study was between 1 and 50. Next, the MA started to denoise the measured signal with AWGN whereby the superimpose layer of a specific length was moved across the measured data with AWGN point while the average was determined and the computation time stop as seen in Equation (2) where i = (1, 2…n), x is the measured signal with AWGN of electrical and acoustic emission PD signals measurement data and z is number of superimpose layer [13, 14].

$$y(i) = \frac{1}{z}\Big(x(i) + x(i-1) + \cdots + x\big(i-(-1)\big)\Big) \quad (2)$$

2.4.2. Finite Impulse Response Filter

The FIR filter advantage is the characteristic of a versatile linear phase filter, which plays a crucial role to maintain the waveform integrity of the original signals [38-40]. FIR type of either LPF or HPF was selected to denoise electrical and acoustic emission PD signals with AWGN as seen in Equation (3) where N is the filter order with coefficient number of N+1.

$$H(z) = \sum_{n=0}^{N} h(n) z^{-n}, n = 0, 1, \ldots, N \quad (3)$$

The Nyquist and cut-off frequency were normalized whereby 1 corresponded to half the sampling rate. The frequency of the measured signal could be up to 4 kHz, which corresponded to a Nyquist frequency of 2 kHz. The noise floor and cut-off frequency were adjusted between 0 and 1. The cut-off frequencies for LPF and HPF were set to 0.15/Π and 0.25/Π [41]. In total, 4 types of the FIR windows were examined known as Chebyshev, Blackman, Hanning, and Hamming. For LPF, FIR Blackman was chosen as the window type in this study [42]. Blackman has a better NCC as compared to Chebyshev, Hanning, and Hamming. The Blackman's computation time was 0.06 s faster than Hanning's and 0.06 s slower than Hamming's. For HPF, the Chebyshev window was selected since Chebyshev had better RNL as compared to Blackman, Hanning, and Hamming. Next, FIR were examined with an interval of 2 up to 100 order numbers.

2.4.3. Discrete Wavelet Transform

The time and scale were used to analyze the electrical and acoustic emission PD signals in DWT. The effective frequency of the mother wavelet was related to the scale domain. Both of LPF and HPF were used to process the measured signal with AWGN, s, as shown in Figure 4. The output of an LPF (L) is the "approximation", which represents the low-frequency content within the measured signal with AWGN band. The output of a HPF (H) is the "detail," which represents the high-frequency content within the measured signal with AWGN band [5], [43].

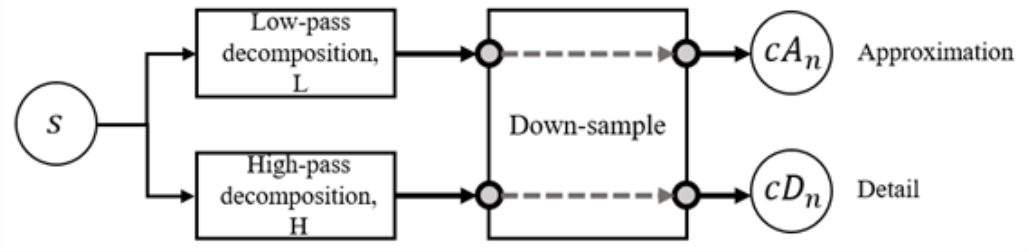

Figure 4. DWT coefficient algorithm architecture

DWT basic working principle is based on the signal denoising window within the samples size. It employs sequences of LPF and HPF to process the time domain signal. LPF shows a low-frequency information known as approximation coefficients, *cA*, while HPF provides a high-frequency information known as detail coefficients, *cD* [44]. In order to obtain detail and approximation coefficients, the time domain of the original signal was processed through a series of HPF and down-sampled by 2 at various scales [45]. It is found that cD_8, cD_9 and cD_{10} were able to denoise electrical and acoustic emission PD signals. Therefore, these *cD* orders with Haar wavelet function were chosen in this study [36]. Overall, DWT has the highest number of the denoising process flow followed by FIR and MA.

2.4.4. Evaluation Method

Electrical and acoustic emission PD signals were analyzed in term of RNL, NCC, NRMSE and computation time [24], [27], [46]. NRMSE and NCC were applied so that the denoised electrical and acoustic emission PD signals with AWGN by each of the methods were in the same scale. Parameter *x* in Equation (4), (5), and (6) is the measured signal with AGWN of electrical and acoustic emission PD signals whereby *y* is the denoised signal, *i* is the number of sample, *N* is the total number of sample and μ is the mean for measured signal with AWGN. The computation time was evaluated based on elapsed time of denoising process between the states to call the measured signal with AWGN until the end of denoising process. The coefficient of variation, C_v was carried to determine the performance of denoising methods studied based on RNL, NCC, NRMSE as shown in Equation (7) [6], [47-48]. The SD is the standard deviation and M is the dataset mean.

$$R\text{NL} = 10\log\frac{1}{N}\sum_{i=1}^{N}\big(x(i) - y(i)\big)^2 \tag{4}$$

Normalized correlation of coefficient (NCC):

$$NCC = \frac{\sum_{i=1}^{N} x(i)*y(i)}{\sqrt{\left(\sum_{i=1}^{N} x(i)^2\right)*\left(\sum_{i=1}^{N} y(i)^2\right)}} \tag{5}$$

Normalized root mean square error (NRMSE):

$$NRMSE = \sqrt{\frac{(x(i)-y(i))^2}{(x(i)-\mu x(i))^2}} \tag{6}$$

Coefficient of variation, C_v:

$$C_v = \frac{SD}{M} \tag{7}$$

3. RESULTS AND DISCUSSION

3.1. Denoising Based on Moving Average

The MA superimpose layers between 10 and 30 are found to have the best NRMSE and RNL to denoise the electrical and acoustic emission PD signals shown in Figures 5 (a) and (b). The peak voltage signals are 9.12 mV and 14 mV for electrical and acoustic emission PD signals. The durations of the denoised electrical and acoustic emission PD signals are 71 ns and 727 µs, respectively.

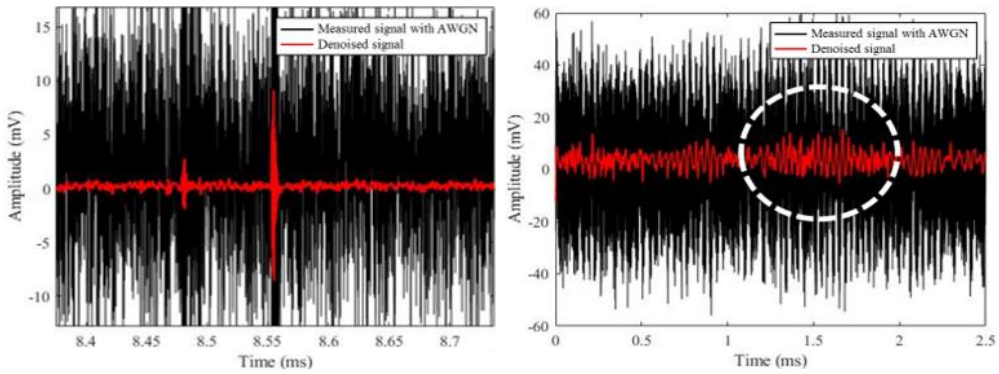

(a) (b)

Figure 5. Denoised (a) electrical and (b) acoustic emission PD signals based on MA

The RNL index for denoising of the electrical PD signal based on the MA is between 34 and 37 while the NRMSE index is between 0.95 and 1 as seen in Figure 6 (a) and (b). The NCC index is between 0.3 and 0.7 as shown in Figure 6(c). In addition, there are 2 regions of computation times are found. The 1st region is between 0.02 s and 0.03 s while the 2nd region is close to 0.04 s as seen in Figure 6(d).

The denoising of the acoustic emission PD signal based on the MA superimpose layers between 10 and 30 result in RNL index in the range between 50 and 70. The NRMSE is between 0.75 and 0.8 as shown in Figures 6 (a) and (b). The NCC index is found between 0.783 and 0.791, as seen in Figures 6 (a) and (c). The computation time is between 0.03 s and 0.04 s as shown in Figure 6(d).

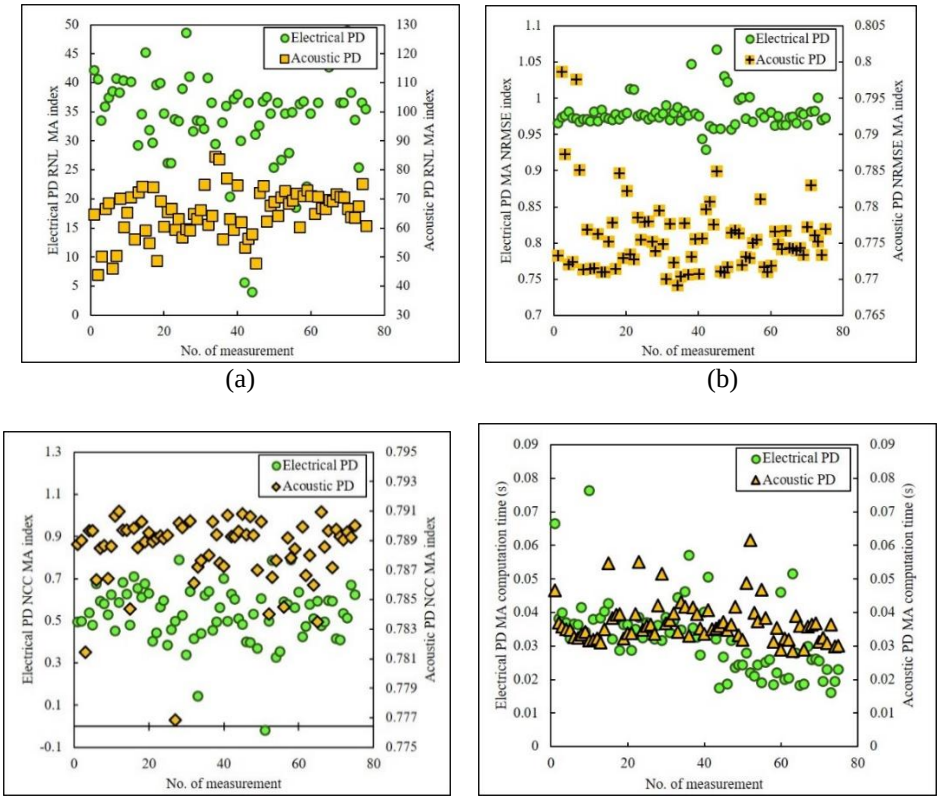

(a) (b)

(c) (d)

Figure 6. (a) RNL index, (b) NRMSE index, (c) NCC index and (d) computation time for denoising of electrical and acoustic emission PD signals based on moving average

3.2. Denoising Based on Finite-Duration Impulse Response (FIR)

The LPF function is able to reduce the high frequency component and let the low frequency to pass. An example of denoised electrical and acoustic emission PD peak voltage signals based on the LPF with

amplitudes of 8.75 mV and 25.3 mV is shown in Figures 7 (a) and (b). The durations to denoise the electrical and acoustic emission PD signals based on LPF are 4.1 ns and 664.35 µs.

The denoising of the electrical PD signal based on the LPF results in RNL index in the range between 15.7 and 35.5 as seen in Figure 8(a), The NRMSE index is from 1.06 to 1.02 as shown in Figure 8(b). The NCC index is between -0.1 and 0.1.

The denoising of the acoustic emission PD signal based on the LPF leads to the RNL index in the range from 40 to 75, whereby the NRMSE index is from 0.82 to 0.83, as shown in Figures 8 (a) and (b). The NCC index is between 0.8 and 0.85. The computation time to denoise both electrical and acoustic emission PD signals is between 0.04 s and 0.05 s.

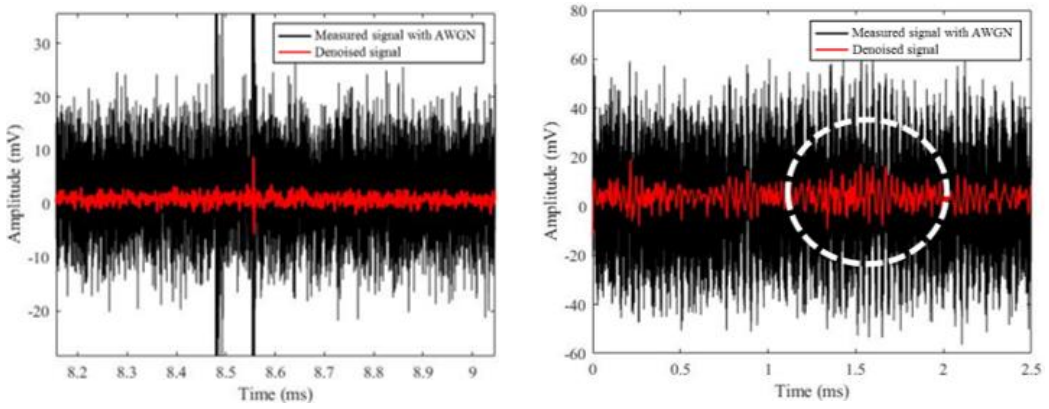

Figure 7. Denoised (a) electrical and (b) acoustic emission PD signals based on finite-duration impulse response low-pass filter

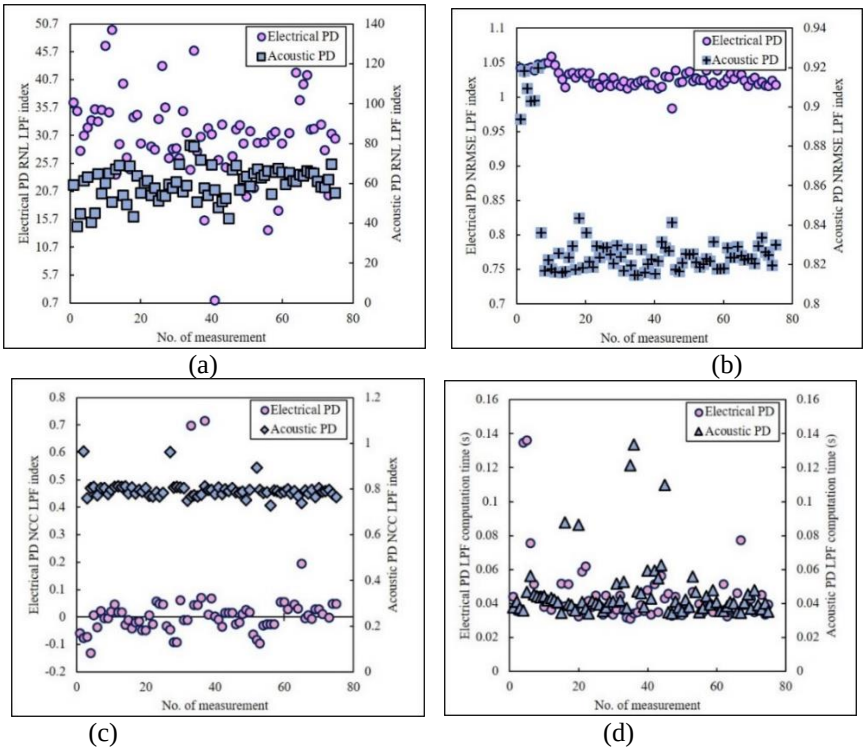

Figure 8. (a) RNL index, (b) NRMSE index, (c) NCC index and (d) computation time for denoising of electrical and acoustic emission PD signals based on finite-duration impulse response low-pass filter

An example for electrical and acoustic emission PD signals denoised based on HPF is shown in Figures 9 (a) and (b). The peak voltage for denoised electrical PD signal is 75.56 mV with the duration of 109 ns. The denoised peak voltage signal and duration for acoustic emission PD are 25.3 mV and 817.97 µs.

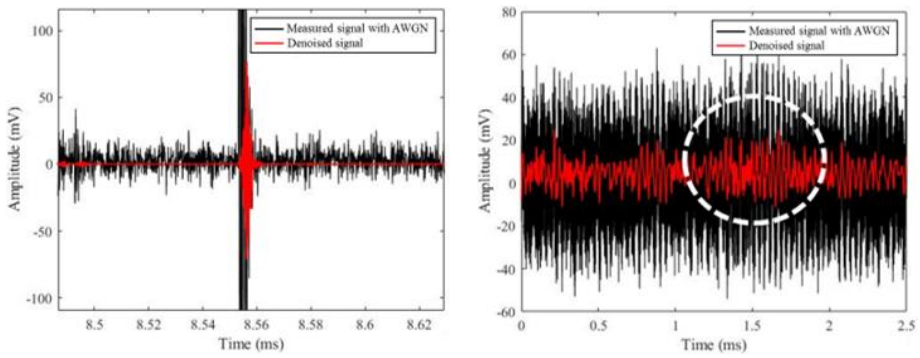

Figure 9. Denoised (a) electrical and (b) acoustic emission PD signals based on finite-duration impulse response high-pass filter

The denoising of electrical PD signal based on HPF leads to the RNL index in the range between 30.5 and 31 as shown in Figure 10(a). The NRMSE index maintains close to 1.04 whereby the NCC index scatters between -0.1 and 0.1 as seen in Figures 10 (b) and (c). The mean for computation time is between 0.04 s and 0.05 s.

The denoising of the acoustic emission PD signal based on HPF results in RNL index in the range from 59.6 to 61.4 while the NRMSE index is between 0.828 and 0.38 as shown in Figures 10 (a) and (b). The NCC index scatters in 2 regions where the 1st region is between 0.65 and 0.68 and the 2nd region is between 0.69 and 0.7 as seen in Figure 10(c). The mean computation times is 0.04 s.

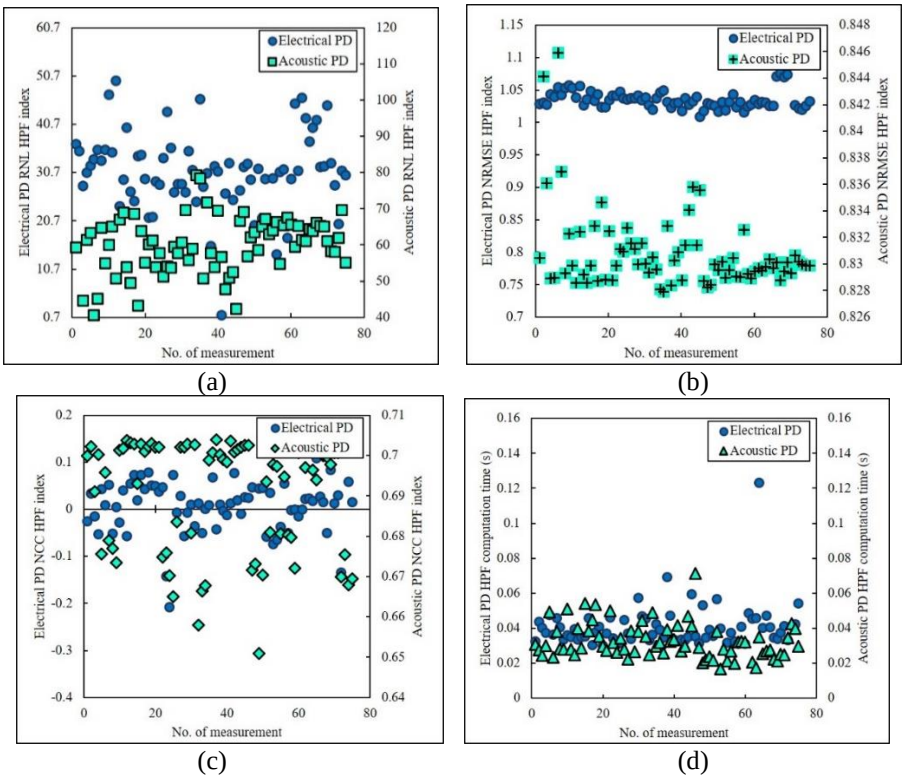

Figure 10. (a) RNL index, (b) NRMSE index, (c) NCC index and (d) computation time for denoising of electrical and acoustic emission PD signals based on finite-duration impulse response high-impulse filter

3.3. Denoising Based on Discrete Wavelet Transform

The RNL and NRMSE indexes as result from the denoising of the electrical PD signal based on DWT are quite similar. cD_{10} has the lowest mean computation time and high NCC index. Similarly, cD_{10} has the lowest computation time for denoising of the acoustic emission PD signal. However, the highest index is NRMSE for cD_{10}. The mean NCC index for cD_{10} is the highest as compared to cD_8 and cD_9. Based on the analyses, cD_{10} is chosen as the detail coefficient for the analyses based on DWT. An example of denoised

electrical and acoustic emission PD signals based on DWT is shown in Figures 11 (a) and (b). The denoised electrical and acoustic emission PD peak voltage signals for DWT cD_{10} are 1.69 mV and 15.2 mV, respectively. The duration to denoise electrical and acoustic emission PD signal based on DWT are 129 ns and 546 µs.

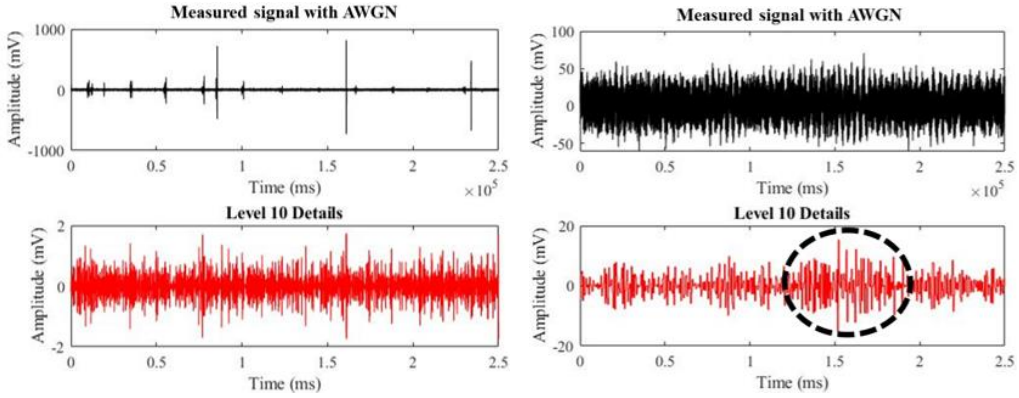

(a) (b)

Figure 11. Denoised (a) electrical and (b) acoustic emission PD signals based on discrete wavelet transform at cD_{10}

The denoising of the electrical PD signal based on DWT results in RNL index in the range from 140 to 180, as shown in Figure 12(a). The NRMSE index is close to 1 as seen in Figure 12(b). The NCC index is scattered in 2 regions where the 1st region is between 0.02 and 0.03 and the 2nd region is between 0.05 and 0.07 as seen in Figure 12(c).

The denoising of the acoustic emission PD signal based on DWT leads to the RNL index close to 200 as shown in Figure 12(a). The NRMSE index is between 0.92 and 0.96 while the NCC index is between 0.3 and 0.4, as seen in Figures 12 (b) and (c). The mean computation times to denoise both electrical and acoustic emission PD signals based on DWT are 0.18 s and 0.22 s.

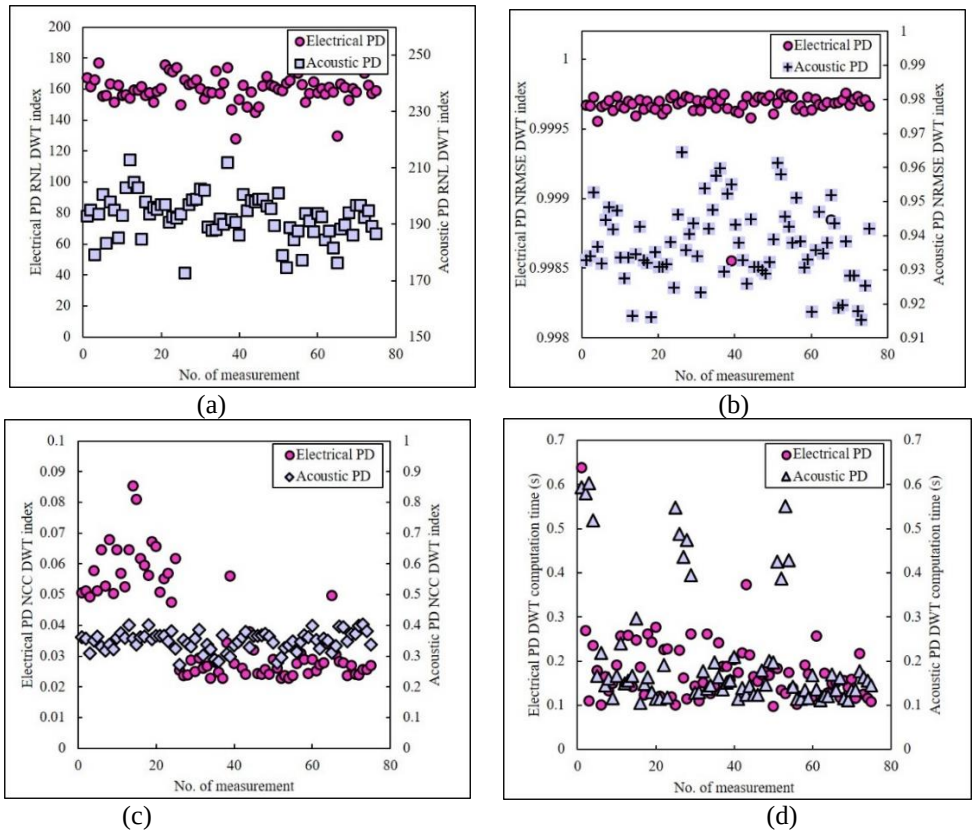

(a) (b)

(c) (d)

Figure 12. (a) RNL index, (b) NRMSE index, (c) NCC index and (d) computation time for denoising of electrical and acoustic emission PD signals based on discrete wavelet transform

3.4. Performance Evaluation of Denoising Methods

Overall, the denoising for both electrical and acoustic emission PD signals based on DWT lead to the highest mean RNL index as shown in Table 2. The RNL index for electrical PD signal is between 30 and 160 [24], [49]. However, LPF results in the highest mean NCC index. The denoising of electrical PD signal based on LPF leads to the lowest NRMSE index. HPF has the lowest NRMSE index for denoising of acoustic emission PD signal. MA has the fastest computation time to denoise both electrical and acoustic emission PD signals [27-28]. The NCC index for electrical PD signal is between 0.006 and 0.793, that is comparable with [50].

Table 2. Mean denoising index and computation time for electrical and acoustic emission PD signals

PD signal	Denoising method	RNL	NCC	NRMSE	Computation time (s)
Electrical	MA	35.671	0.530	0.980	0.032
	LPF	59.645	0.793	0.830	0.045
	HPF	30.561	0.006	1.036	0.042
	DWT	160.172	0.038	1.000	0.179
Acoustic emission	MA	65.173	0.788	0.776	0.038
	LPF	59.645	0.793	0.830	0.046
	HPF	59.658	0.691	0.831	0.038
	DWT	192.492	0.349	0.937	0.218

Generally, the denoising for both electrical and acoustic emission PD signals based on HPF lead to the highest RNL C_v index as seen in Table 3. The denoising of electrical PD signal based on HPF leads to the highest NCC C_v index. DWT has the highest NCC C_v index for denoising acoustic emission PD signal. The lowest NRMSE C_v index is found for denoising of electrical PD signal based on DWT. The lowest NRMSE C_v index for denoising of acoustic emission PD signal is found for HPF. MA has the fastest computation time to denoise both electrical and acoustic emission PD signals based on C_v index.

Table 3. Coefficient of variation for mean denoising index

PD signal	Denoising method	RNL	NCC	NRMSE	Computation time
Electrical	MA	0.248	0.247	0.023	0.337
	LPF	0.131	0.045	0.029	0.496
	HPF	0.284	9.479	0.014	0.460
	DWT	0.055	0.431	0.000	0.428
Acoustic emission	MA	0.123	0.003	0.007	0.270
	LPF	0.131	0.045	0.029	0.395
	HPF	0.135	0.020	0.004	0.308
	DWT	0.040	0.086	0.012	0.691

4. CONCLUSION

According to the current study, it is found that the MA superimpose layers between 10 and 30 are optimum to denoise both electrical and acoustic emission PD signals based on RNL and NRMSE indexes. The 48th order number of HPF has the best denoising NCC index whereby RNL and NRMSE indexes are close to each other. For LPF, the 70th order number has the optimum mean RNL and NRMSE denoising indexes. The denoising of both electrical and acoustic emission PD signals based on HPF results in the highest RNL C_v index. HPF can also lead to the highest NCC C_v index through denoising of electrical PD signal. The lowest NRMSE C_v index is achieved once the denoising of electrical and acoustic emission PD signals are carried by DWT and HPF. Overall C_v indexes indicate that DWT and MA denoising perform better to denoise electrical and acoustic emission PD signals. The DWT has a low NRMSE C_v index and high RNL C_v index as a result from the denoising electrical PD signal. The MA has a low NCC and computation time C_v index for the acoustic emission PD signal followed by LPF, DWT and HPF.

ACKNOWLEDGMENTS

This research was funded by Matching Grant Universiti Putra Malaysia – Kyushu Institute of Technology (UPM.RMC/800/2/2/4/Matching UPM – KYUTECH/2021/ 9300481).

REFERENCES

[1] R. Hussein, K. B. Shaban, and A. H. El-Hag, "Denoising different types of acoustic partial discharge signals using power spectral subtraction," *Inst. Eng. Technol. High Volt.*, vol. 3, no. 1, pp. 44–50, 2018, doi: 10.1049/hve.2017.0119.

[2] M. Ghorat, G. B. Gharehpetian, H. Latifi, and M. A. Hejazi, "A new partial discharge signal denoising algorithm based on adaptive dual-tree complex wavelet transform," *IEEE Trans. Instrum. Meas.*, vol. 67, no. 10, pp. 2262–2272, 2018, doi: 10.1109/TIM.2018.2816438.

[3] Y. O. Shaker, "Detection of partial discharge acoustic emission in power transformer," *Int. J. Electr. Comput. Eng.*, vol. 9, no. 6, pp. 4573–4579, 2019, doi: 10.11591/ijece.v9i6.pp4573-4579.

[4] [4] S. Coenen, S. Kornhuber, A. Müller, and M. Beltle, "Uhf and Acoustic Partial Discharge Localisation in Power Transformers," *XVI Int. Symp. High Volt. Eng. Hann. Ger. August 22-26, 2011*, no. October 2014, p. D-015, 1-6, 2011.

[5] N. A. Yusoff *et al.*, "Denoising technique for partial discharge signal : A comparison performance between artificial neural network, fast fourier transform and discrete wavelet transform," *PECON 2016 - 2016 IEEE 6th Int. Conf. Power Energy, Conf. Proceeding*, pp. 311–316, 2017, doi: 10.1109/PECON.2016.7951579.

[6] G. Chen, J. Tao, Y. Ma, H. U. I. Fu, Y. Liu, and Z. Zhou, "On-site Portable Partial Discharge Detection Applied to Power Cables Using HFCT and UHF methods 3 Portable PD Monitoring Device," *On-site Portable Partial Disch. Detect. Appl. to Power Cables Using HFCT UHF methods*, vol. 15, pp. 83–90, 2016.

[7] K. Zhou, M. Li, Y. Li, M. Xie, and Y. Huang, "An improved denoising method for partial discharge signals contaminated by white noise based on adaptive short-time singular value decomposition," *Energies*, vol. 12, no. 18, 2019, doi: 10.3390/en12183465.

[8] A. A. Soltani and A. El-Hag, "A new radial basis function neural network-based method for denoising of partial discharge signals," *Meas. J. Int. Meas. Confed.*, vol. 172, no. January, p. 108970, 2021, doi: 10.1016/j.measurement.2021.108970.

[9] Y. Wang, P. Chen, Y. Zhao, and Y. Sun, "A Denoising Method for Mining Cable PD Signal Based on Genetic Algorithm Optimization of VMD and Wavelet Threshold," *Sensors*, vol. 22, no. 23, 2022, doi: 10.3390/s22239386.

[10] H. Janani, S. Shahabi, and B. Kordi, "Separation and Classification of Concurrent Partial Discharge Signals Using Statistical-Based Feature Analysis," *IEEE Trans. Dielectr. Electr. Insul.*, vol. 27, no. 6, pp. 1933–1941, 2020, doi: 10.1109/TDEI.2020.009043.

[11] J. Rubio-Serrano, J. E. Posada, and J. A. Garcia-Souto, "Detection and location of acoustic and electric signals from partial discharges with an adaptative wavelet-filter denoising," in *Electrical Engineering and Applied Computing, Lecture Notes in Electrical Engineering*, 2011, pp. 25–38. doi: 10.1007/978-94-007-1192-1_3.

[12] H. Mohamed *et al.*, "Partial discharge localization based on received signal strength," *ICAC 2017 - 2017 23rd IEEE Int. Conf. Autom. Comput. Addressing Glob. Challenges through Autom. Comput.*, no. September, pp. 7–8, 2017, doi: 10.23919/IConAC.2017.8082028.

[13] R. Sarathi, P. D. Singh, and M. G. Danikas, "Characterization of partial discharges in transformer oil insulation under AC and DC voltage using acoustic emission technique," *J. Electr. Eng.*, vol. 58, no. 2, pp. 91–97, 2007.

[14] R. Ghosh, B. Chatterjee, and S. Dalai, "A new method for the estimation of time difference of arrival for localization of partial discharge sources using acoustic detection technique," in *2016 IEEE 7th Power India International Conference, PIICON 2016*, Bikaner, India: IEEE, 2017, pp. 1–5. doi: 10.1109/POWERI.2016.8077180.

[15] H. Dadashi Ilkhechi, M. H. Samimi, and R. Yousefvand, "Generation of acoustic phase-resolved partial discharge patterns by utilizing UHF signals," *Int. J. Electr. Power Energy Syst.*, vol. 113, no. January, pp. 906–915, 2019, doi: 10.1016/j.ijepes.2019.06.018.

[16] M. S. A. Rahman, P. L. Lewin, and P. Rapisarda, "Autonomous localization of partial discharge sources within large transformer windings," *IEEE Trans. Dielectr. Electr. Insul.*, vol. 23, no. 2, pp. 1088–1098, 2016, doi: 10.1109/TDEI.2015.005070.

[17] P. Kailasapathi and D. Sivakumar, "ANALYZING POWER QUALITY DISTURBANCES USING DIFFERENT WAVELET FAMILIES," *Glob. J. Engg. Appl. Sci. 2013 3*, vol. 3, no. 1, pp. 8–13, 2013.

[18] C. Boya, M. Ruiz-Llata, J. Posada, and J. A. Garcia-Souto, "Identification of multiple partial discharge sources using acoustic emission technique and blind source separation," *IEEE Trans. Dielectr. Electr. Insul.*, vol. 22, no. 3, pp. 1663–1673, 2015, doi: 10.1109/TDEI.2015.7116363.

[19] T. Boczar, S. Borucki, A. Cichoń, and D. Zmarzły, "Application possibilities of artificial neural networks for recognizing partial discharges measured by the acoustic emission method," *IEEE Trans. Dielectr. Electr. Insul.*, vol. 16, no. 1, pp. 214–223, 2009, doi: 10.1109/TDEI.2009.4784570.

[20] X. Zhou, C. Zhou, and I. J. Kemp, "An improved methodology for application of wavelet transform to partial discharge measurement denoising," *IEEE Trans. Dielectr. Electr. Insul.*, vol. 12, no. 3, pp. 586–594, 2005, doi: 10.1109/TDEI.2005.1453464.

[21] E. Agletdinov, D. Merson, and A. Vinogradov, "A new method of low amplitude signal detection and its application in acoustic emission," *Appl. Sci.*, vol. 10, no. 1, pp. 1–14, 2020, doi: 10.3390/app10010073.

[22] R. Hussein, K. B. Shaban, and A. H. El-Hag, "Wavelet Transform with Histogram-Based Threshold Estimation for Online Partial Discharge Signal Denoising," *IEEE Trans. Instrum. Meas.*, vol. 64, no. 12, pp. 3601–3614, 2015, doi: 10.1109/TIM.2015.2454651.

[23] Q. Lin, F. Lyu, S. Yu, H. Xiao, and X. Li, "Optimized Denoising Method for Weak Acoustic Emission Signal in Partial Discharge Detection," *IEEE Trans. Dielectr. Electr. Insul.*, vol. 29, no. 4, pp. 1409–1416, Aug. 2022, doi: 10.1109/TDEI.2022.3183662.

[24] R. Hussein, K. B. Shaban, and A. H. El-Hag, "Energy conservation-based thresholding for effective wavelet denoising of partial discharge signals," *IET Sci. Meas. Technol.*, vol. 10, no. 7, pp. 813–822, 2016, doi: 10.1049/iet-smt.2016.0168.

[25] T. Jin, Q. Li, and M. A. Mohamed, "A Novel Adaptive EEMD Method for Switchgear Partial Discharge Signal Denoising," *IEEE Access*, vol. 7, pp. 58139–58147, 2019, doi: 10.1109/ACCESS.2019.2914064.

[26] D. Ambika and V. Radha, "A comparative study between Discrete Wavelet Transform and Linear Predictive Coding," in *Proceedings of the 2012 World Congress on Information and Communication Technologies, WICT 2012*, 2012, pp. 965–969. doi: 10.1109/WICT.2012.6409214.

[27] J. Baili, S. Lahouar, M. Hergli, I. L. Al-Qadi, and K. Besbes, "GPR signal de-noising by discrete wavelet transform," *NDT&E Int.*, vol. 42, no. 8, pp. 696–703, 2009, doi: 10.1016/j.ndteint.2009.06.003.

[28] J. Melchiorre, A. Manuello Bertetto, M. M. Rosso, and G. C. Marano, "Acoustic Emission and Artificial Intelligence Procedure for Crack Source Localization," *Sensors*, vol. 23, no. 2, Jan. 2023, doi: 10.3390/s23020693.

[29] B. Standard, "High-voltage test techniques - Partial discharge measurements," *Eur. Comm. Electrotech. Stand.*, no. 3rd Edition, 2000, doi: 10.1049/joe.2018.0172.

[30] N. Pattanadech and M. Muhr, "Comments on PDIV testing procedure according to IEC 61294," in *2017 IEEE 19th International Conference on Dielectric Liquids, (ICDL), Manchester, United Kingdom, 25-29 June, 2017*, 2017, pp. 1–4. doi: 10.1109/ICDL.2017.8124658.

[31] Hyrax Oils Sdn. Bhd., "Hyrax Hypertrans Transformer Oil (IEC 60296 :2020) –Edition 5," Kuala Lumpur, 2020.

[32] F. Sipahutar *et al.*, "Ramp Rates Effect in Ramp Method for Partial Discharge Inception Voltage Measurement in Mineral Oil Effects of thermal aging on Dielectric Properties and DGA of oil-paper insulations View project The 4th International Conference on Electrical Engineering and Informatics (ICEEI 2013) Ramp Rates Effect in Ramp Method for Partial Discharge Inception Voltage Measurement in Mineral Oil ScienceDirect," *Procedia Technol.*, vol. 11, pp. 608–613, 2013, doi: 10.1016/j.protcy.2013.12.235.

[33] N. A. Mohamad, N. Azis, J. Jasni, M. Zainal, A. Ab, and R. Yunus, "Experimental Study on the Partial Discharge Characteristics of Palm Oil and Coconut Oil based Al 2 O 3 Nanofluids in the Pres- ence of Sodium Dodecyl Sulfate," pp. 1–19, 2021.

[34] Y. W. Tang, C. C. Tai, C. C. Su, C. Y. Chen, and J. F. Chen, "A correlated empirical mode decomposition method for partial discharge signal denoising," *Meas. Sci. Technol.*, vol. 21, no. 8, 2010, doi: 10.1088/0957-0233/21/8/085106.

[35] IEEE, "IEEE Guide for the Detection, Location and Interpretation of Sources of Acoustic Emissions from Electrical Discharges in Power Transformers and Power Reactors," 2018. doi: 10.1109/IEEESTD.2019.8664690.

[36] A. H. Mohd Hashim *et al.*, "Partial Discharge Localization in Oil Through Acoustic Emission Technique Utilizing Fuzzy Logic," *IEEE Trans. Dielectr. Electr. Insul.*, vol. 29, no. 2, pp. 623–630, 2022, doi: 10.1109/TDEI.2022.3157911.

[37] K. Ibrahim, R. M. Sharkawy, M. M. A. Salama, and R. Bartnikas, "Realization of Partial Discharge Signals in Transformer Oils Utilizing Advanced Computational Techniques," 2012.

[38] L. Litwin, "FIR and IIR digital filters," *IEEE Potentials*, vol. 19, no. 4, pp. 28–31, 2000, doi: 10.1109/45.877863.

[39] L. Song, "Position location of partial discharges in power transformers using fiber acoustic sensor arrays," *Opt. Eng.*, vol. 45, no. 11, p. 114401, 2006, doi: 10.1117/1.2390681.

[40] M. Quizhpi-Cuesta, F. Gómez-Juca, W. Orozco-Tupacyupanqui, and F. Quizhpi-Palomeque, "An alternative method for Partial Discharges measurement using digital filters," *2017 10th Int. Symp. Adv. Top. Electr. Eng. ATEE 2017*, pp. 92–97, 2017, doi: 10.1109/ATEE.2017.7905172.

[41] S. Sriram, S. Nitin, K. M. M. Prabhu, and M. J. Bastiaans, "Signal denoising techniques for partial discharge measurements," *IEEE Trans. Dielectr. Electr. Insul.*, vol. 12, no. 6, pp. 1182–1191, 2005, doi: 10.1109/TDEI.2005.1561798.

[42] S. Chakraborty, "Advantages of Blackman Window over Hamming Window Method for designing FIR Filter," *Int. J. Comput. Sci. Eng. Technol.*, vol. 4, no. 08, pp. 1181–1189, 2013, [Online]. Available: http://ijcset.com/docs/IJCSET13-04-08-030.pdf

[43] A. Swedan, A. H. El-Hag, and K. Assaleh, "Acoustic detection of partial discharge using signal processing and pattern recognition techniques," *Insight Non-Destructive Test. Cond. Monit.*, vol. 54, no. 12, pp. 667–672, 2012, doi: 10.1784/insi.2012.54.12.667.
[44] M. Harbaji, K. Shaban, and A. El-Hag, "Classification of common partial discharge types in oil-paper insulation system using acoustic signals," *IEEE Trans. Dielectr. Electr. Insul.*, vol. 22, no. 3, pp. 1674–1683, 2015, doi: 10.1109/TDEI.2015.7116364.
[45] Y. Xie, J. Tang, and Q. Zhou, "Suppressing white-noise in partial discharge measurements—part 1: construction of complex Daubechies wavelet and complex threshold," *Eur. Trans. Electr. POWER 2010*, vol. 20, no. June 2009, pp. 800–810, 2009, doi: 10.1002/etep.
[46] S. M. Joseph, F. S. A, and B. A. P, "Comparing Speech Compression Using Waveform Coding and Parametric Coding," *Int. J. Electron. Eng.*, vol. 3, no. 1, pp. 35–38, 2011.
[47] W. Chen, "Importance Evaluation Method on the Fault Modes of Power Transformer Based on Trapezoidal Fuzzy Number," no. Ii, pp. 5–6, 2012.
[48] Y. V. Thien *et al.*, "Investigation on the lightning breakdown voltage of Palm Oil and Coconut Oil under non-uniform field," *Conf. Proceeding - 2014 IEEE Int. Conf. Power Energy, PECon 2014*, no. November, pp. 1–4, 2014, doi: 10.1109/PECON.2014.7062402.
[49] B. Vigneshwaran, R. V. Maheswari, and P. Subburaj, "An improved threshold estimation technique for partial discharge signal denoising using Wavelet Transform," *Proc. IEEE Int. Conf. Circuit, Power Comput. Technol. ICCPCT 2013*, pp. 300–305, 2013, doi: 10.1109/ICCPCT.2013.6528823.
[50] V. C. Thuc and H. S. Lee, "Partial Discharge (PD) Signal Detection and Isolation on High Voltage Equipment Using Improved Complete EEMD Method," *Energies*, vol. 15, no. 16, Aug. 2022, doi: 10.3390/en15165819.

BIOGRAPHY OF AUTHORS

Ahmad Hafiz Mohd Hashim received the B.Eng. degree in electrical power engineering and the M.Eng. degree in manufacturing engineering management from the Universiti Putra Malaysia, Serdang, Malaysia, in 2008 and 2013, respectively. He is currently a Senior Lecturer with the Electrical and Electronic Department of Engineering, German-Malaysian Institute, Kajang, Malaysia. His research interests include condition monitoring for partial discharge in transformers, artificial intelligence, signal processing, and machine learning.

Norhafiz Azis (Senior Member, IEEE) received the B.Eng. degree in electrical and electronic engineering from Universiti Putra Malaysia, Serdang, Malaysia, in 2007 and Ph.D. degree in electrical and electronic engineering related to the power transformer from The University of Manchester, Manchester, U.K, in 2012. He is currently an Associate Professor with the Department of Electrical and Electronic Engineering, Universiti Putra Malaysia. His research interests are in-service aging of transformer insulation, condition monitoring, asset management, and alternative insulation materials for transformers

Jasronita Jasni (Senior Member, IEEE) received the B.Eng. degree in electrical engineering and the M.Eng. degree in electrical engineering from Universiti Teknologi Malaysia, Johor Bahru, Malaysia, in 1998 and 2001, respectively, and the Ph.D. degree in electrical power engineering from Universiti Putra Malaysia, Serdang, Malaysia, in 2010. She is currently an Associate Professor with the Department of Electrical and Electronic Engineering, Universiti Putra Malaysia. Her research interests include power system analysis for static and dynamics, load flow analysis, embedded generation, and renewable energy.

Mohd Amran Mohd Radzi (Senior Member, IEEE) was born in Kuala Lumpur, Malaysia, in 1978. He received the B.Eng. (Hons.) and M.Sc. degrees in electrical power engineering from Universiti Putra Malaysia (UPM), Serdang, Selangor, Malaysia, in 2000 and 2002, respectively, and the Ph.D. degree in power electronics from the University of Malaya (UM), Kuala Lumpur, Malaysia, in 2010. He is currently a Professor with the Department of Electrical and Electronic Engineering and the Deputy Dean of the Faculty of Engineering, UPM. His research and teaching interests are power electronics, power quality, and renewable energy.

Masahiro Kozako (Member, IEEE) received the B.Eng., M.Eng., and Dr. Eng. degrees in electrical engineering from the Kyushu Institute of Technology, Kitakyushu-shi, Japan, in 1997, 1999, and 2002, respectively. He is currently an Associate Professor with the Department of Electrical and Electronic Engineering, Kyusyu Institute of Technology. He worked with Waseda University, Tokyo, Japan, for three years, and the Kagoshima National College of Technology, Kirishima, Japan, for three years, as an Assistant Professor. He was a Visiting Researcher with the LAPLACE, Université Paul Sabatier, Toulouse, France, in 2011. His research interests concern the development of new insulating polymer nanocomposite materials and the development of diagnostic techniques for electric power apparatus. Prof. Masahiro is also a member of the Japan Institute of Electronics Packaging (JIEP), the Institute of Electrical Engineers of Japan (IEEJ), and the Conseil International des Grands Réseaux Electriques or Inter- national Council on Large Electric Systems (CIGRE).

Mohamad Kamarol Mohd Jamil (Senior Member, IEEE) received the B.Eng degree (Hons.) in electrical engineering from Universiti Technology Mara, Shah Alam, Malaysia, in 2000, and the M.Eng. and D.Eng. degrees from Kyushu Institute of Technology, Kitakyushu-shi, Japan, in 2005 and 2008, respectively. He is currently an Associate Professor with the School of Electrical and Electronic Engineering, Universiti Sains Malaysia, Nibong Tebal, Malaysia. He was a Senior Engineer with Sankyo Seiki (M) Sdn. Bhd., Kuala Lumpur, Malaysia, for almost eight years. His research interests include the insulation properties in oil palm and solid dielectric material, insulation properties of environmentally benign gas, PD detection technique for insulation diagnosis of power apparatus, and electrical machine.

Zaini Yaakub received the B.Sc. (AppChem) degree (Hons.) from Sheffield Hallam University, Sheffield, U.K., in 1993. He joined Caleb Brett Malaysia in the same year as a chemist before joining Hyrax Oil Sdn. Bhd, Klang, Malaysia, in 1994. Currently, he is an Assistant General Manager with Hyrax Oil after having had a working experience for more than 20 years on various responsibilities and roles. His research interests are in the field of electrical insulating oils.